Supporting information

Effect of Complexation with *Closo*-Decaborate Anion on Photophysical Properties of Copolyfluorenes Containing Dicyanophenanthrene Units in the Main Chain

Anton A. Yakimanskiy [1], Ksenia I. Kaskevich [1], Tatiana G. Chulkova [1], Elena L. Krasnopeeva [1,*], Serguei V. Savilov [2,3], Vera V. Voinova [3], Nikolay K. Neumolotov [3], Andrey P. Zhdanov [3], Anastasia V. Rogova [4], Felix N. Tomilin [4,5], Konstantin Yu. Zhizhin [3], and Alexander V. Yakimansky [1]

[1] Institute of Macromolecular Compounds RAS, Bolshoi Prospect of Vasilyevsky Island 31, St. Petersburg, 199004, Russia; yakimanskii@gmail.com (A.A.Y.); kaskevich-ksenia@yandex.ru (K.I.K.); tgc@mail.ru (T.G.C.); yakimansky@yahoo.com (A.V.Y.)

[2] Department of Chemistry, Lomonosov Moscow State University, Moscow 119991, Russia; savilov@mail.ru

[3] Kurnakov Institute of General and Inorganic Chemistry RAS, Moscow, 119991, Russia; savilov@mail.ru (S.V.S); veravoinova@rx24.ru (V.V.V.); neumolotovn@gmail.com (N.K.N.); zh_dots@mail.ru (A.P.Z.); zhizhin@igic.ras.ru (K.Y.Z.)

[4] Kirensky Institute of Physics, Federal Research Center KSC SB RAS, Krasnoyarsk 660036, Russia; arogova1927@gmail.com (A.V.R.); felixnt@gmail.com (F.N.T.)

[5] Laboratory for Digital Controlled Drugs and Theranostics, Federal Research Center "Krasnoyarsk Science Center SB RAS", Krasnoyarsk, 660041, Russia; felixnt@gmail.com

* Correspondence: opeeva@gmail.com; Tel.: +7-812-3237407

Table S1. Molecular mass[1] characteristics of copolyfluorenes.

CPF name	Comonomer loading (x), mol%	M_w*10^{-3} g/mol	M_n*10^{-3} g/mol	M_w/M_n
PFCN0.5 [1]	0.5	32.5	20.9	1.55
PFCN2.5 [1]	2.5	11.5	9.0	1.3
PFCN5	5.0	9.5	6.8	1.4

[1] Weight-average molecular weight (M_w), number-average molecular weight (M_n) and molecular weight polydispersity ratio (M_w/M_n) of the samples were estimated by size exclusion chromatography (SEC). LS detector data presented.

Table S2. FT-IR and ^{1}H NMR selected data for synthesized compounds.

name	FT-IR data, cm^{-1}	^{1}H NMR data, ppm
PFCN0.5+B	2921, s (ν_{as} CH_2) 2850, s (ν_s CH_2) 2492.5, m (ν BH) 1456, s (ν_s C-C_{ar}) 810, s (δ CH_{ar})	7.88-7.86 (m, 2H), 7.74-7.70 (m, 4H), H_{ar} fluorene 4.14 (q, *J* = 7.0 Hz), $CH_3C\boldsymbol{H_2}O$- (terminal) 3.32-3.19 (m), $CH_3CH_2CH_2\boldsymbol{CH_2}N$- 2.4-1.8 (m, 4H) CH_2 octyl 1.65 (m), $CH_3CH_2\boldsymbol{CH_2}CH_2N$- 1.54-1.44 (m), $CH_3\boldsymbol{CH_2}CH_2CH_2N$-and $C\boldsymbol{H_3}CH_2O$- (terminal) 1.25-1.17 (m, 20H), CH_2 octyl 1.02 (m), $\boldsymbol{CH_3}CH_2CH_2CH_2N$- 0.86-0.83 (m, 10H), CH_2 and CH_3 octyl
PFCN2.5+B	2922, s (ν_{as} CH_2) 2850, s (ν_s CH_2) 2476, m (ν BH) 1458, s (ν_s C-C_{ar}) 810, s (δ CH_{ar})	7.88-7.86 (m, 2H), 7.74-7.70 (m, 4H), H_{ar} fluorene 4.14 (q, *J* = 7.0 Hz), $CH_3C\boldsymbol{H_2}O$- (terminal) 3.32-3.19 (m), $CH_3CH_2CH_2\boldsymbol{CH_2}N$- 2.4-1.8 (m, 4H) CH_2 octyl 1.65 (m), $CH_3CH_2\boldsymbol{CH_2}CH_2N$- 1.55-1.45 (m), $CH_3\boldsymbol{CH_2}CH_2CH_2N$-and $C\boldsymbol{H_3}CH_2O$- (terminal) 1.25-1.17 (m, 20H), CH_2 octyl 1.02 (t, *J* = 7.3 Hz), $\boldsymbol{CH_3}CH_2CH_2CH_2N$- 0.86-0.83 (m, 10H), CH_2 and CH_3 octyl
PFCN5+B	2923, s (ν_{as} CH_2) 2851, s (ν_s CH_2) 2492.5, m (ν BH) 1457, s (ν_s C-C_{ar}) 811, s (δ CH_{ar})	7.88-7.86 (m, 2H), 7.74-7.70 (m, 4H), H_{ar} fluorene 4.17-4.11. (m), $CH_3C\boldsymbol{H_2}O$- (terminal) 3.32-3.19 (m), $CH_3CH_2CH_2\boldsymbol{CH_2}N$- 2.4-1.8 (m, 4H) CH_2 octyl 1.66 (m), $CH_3CH_2\boldsymbol{CH_2}CH_2N$- 1.54-1.44 (m), $CH_3\boldsymbol{CH_2}CH_2CH_2N$-and $C\boldsymbol{H_3}CH_2O$- (terminal) 1.25-1.16 (m, 20H), CH_2 octyl 1.02 (t, *J* = 7.3 Hz), $\boldsymbol{CH_3}CH_2CH_2CH_2N$- 0.86-0.83 (m, 10H), CH_2 and CH_3 octyl

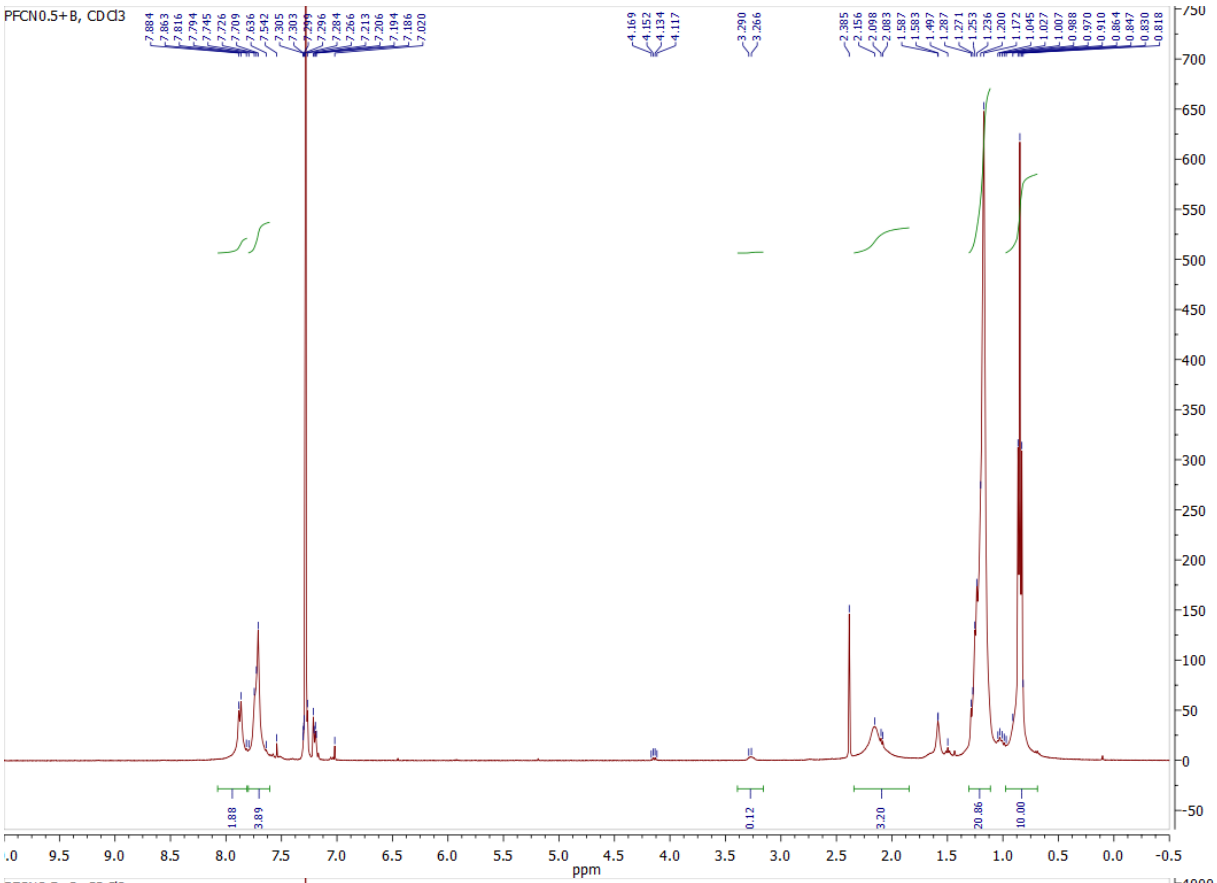
PFCN0.5+B, CDCl3
ppm

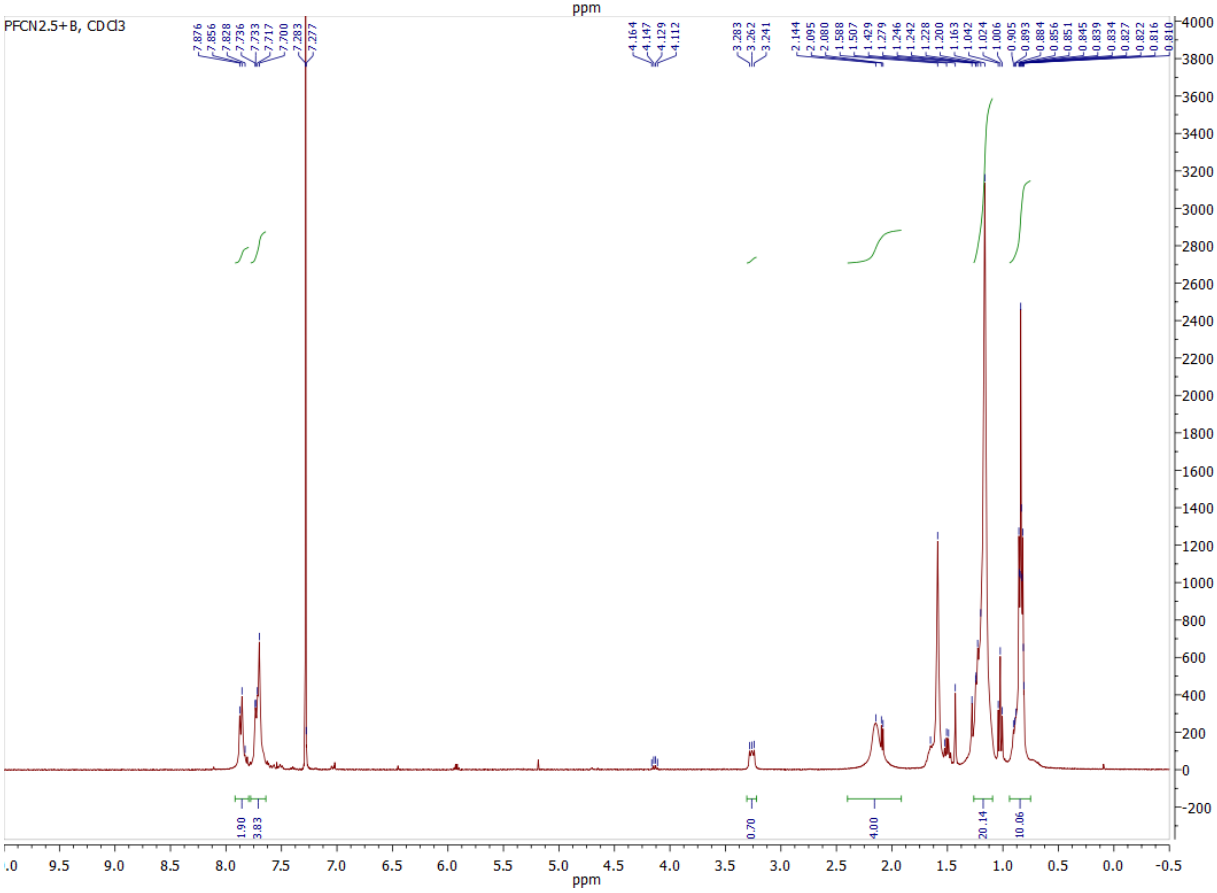
PFCN2.5+B, CDCl3
ppm

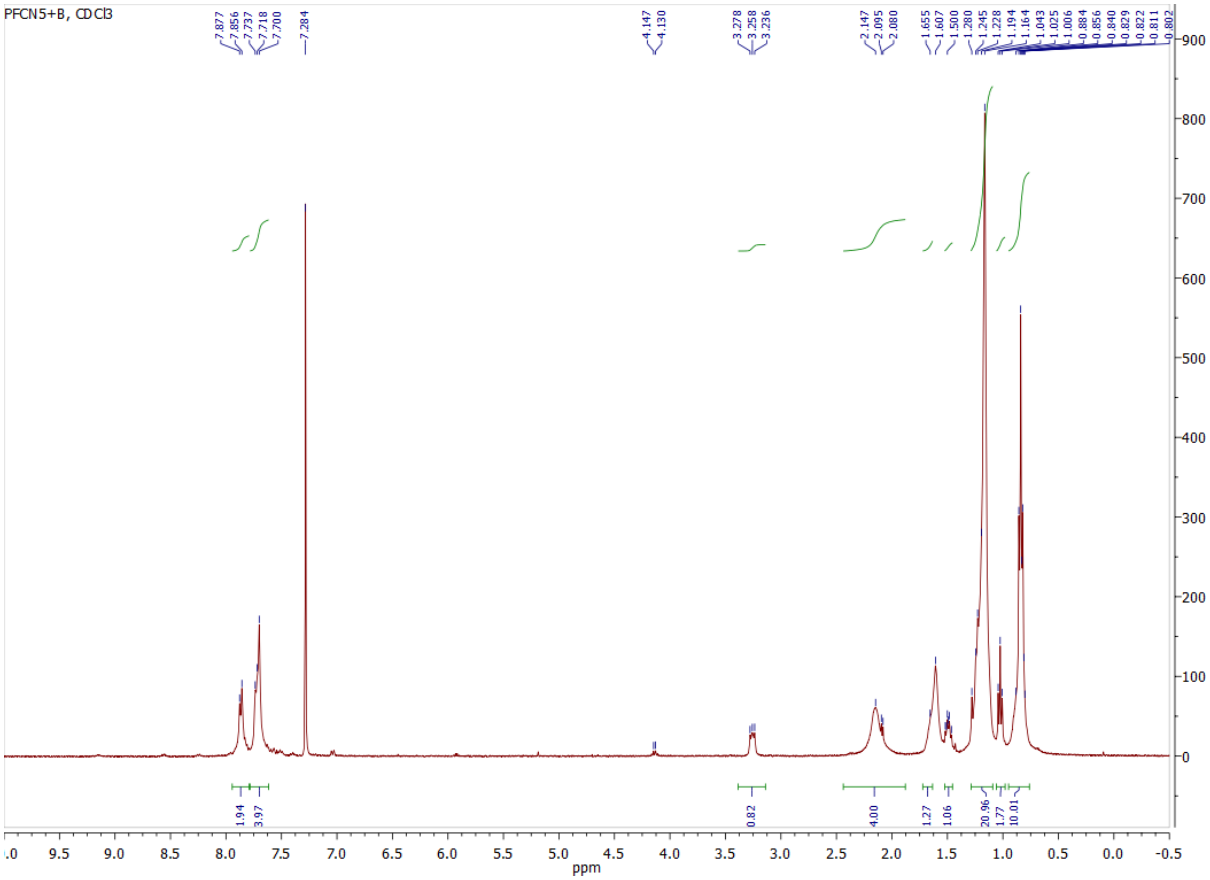

Figure S1. ^{1}H NMR spectra of compounds (PFCN0.5+B, PFCN2.5+B, and PFCN5+B) in $CDCl_3$.

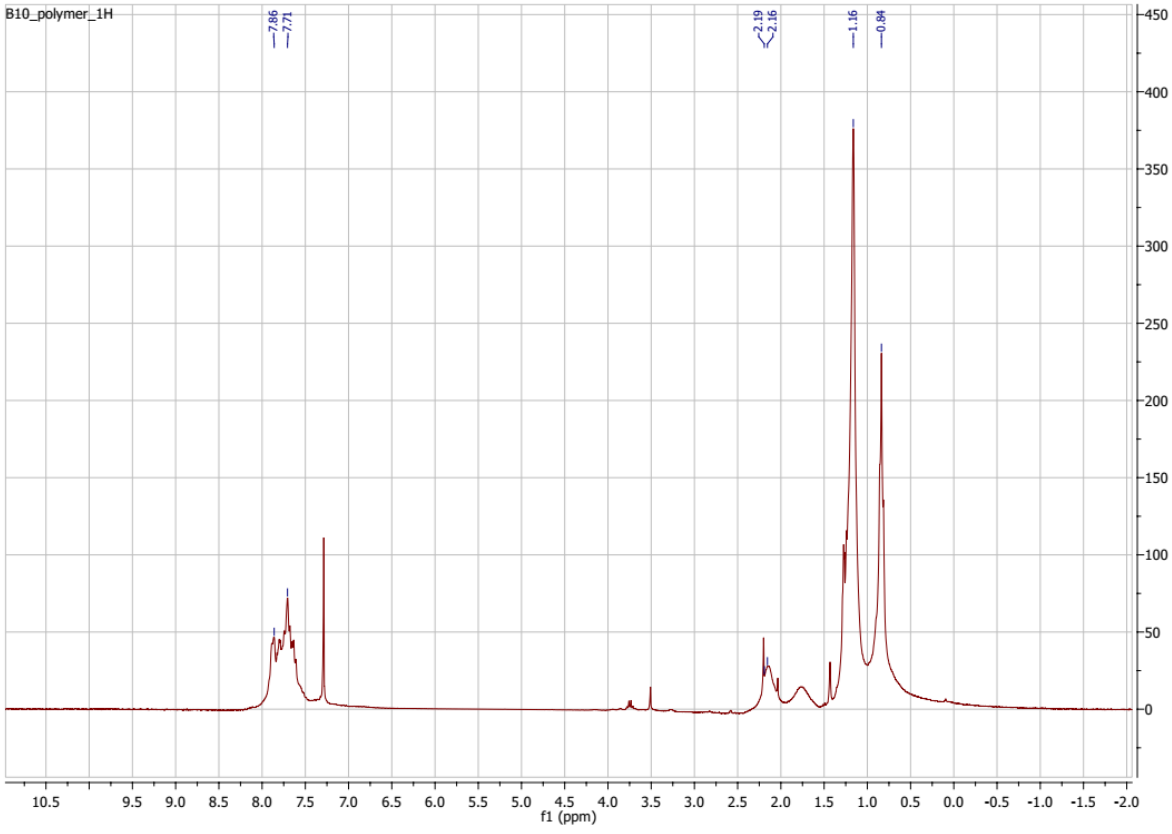

Figure S2. ^{1}H NMR spectrum of PFCN2.5+B′ in $CDCl_3$.

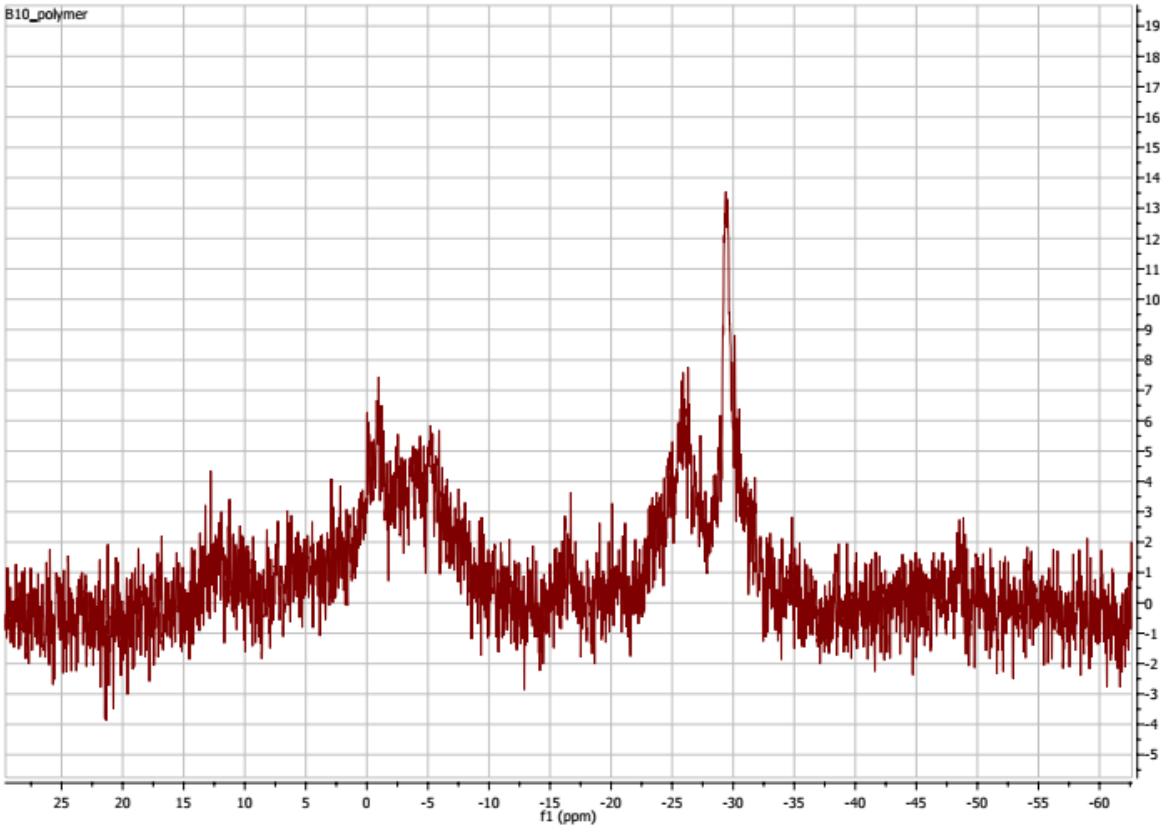

Figure S3. $^{11}B\{^{1}H\}$ NMR spectrum of PFCN2.5+B′ in $CDCl_3$.

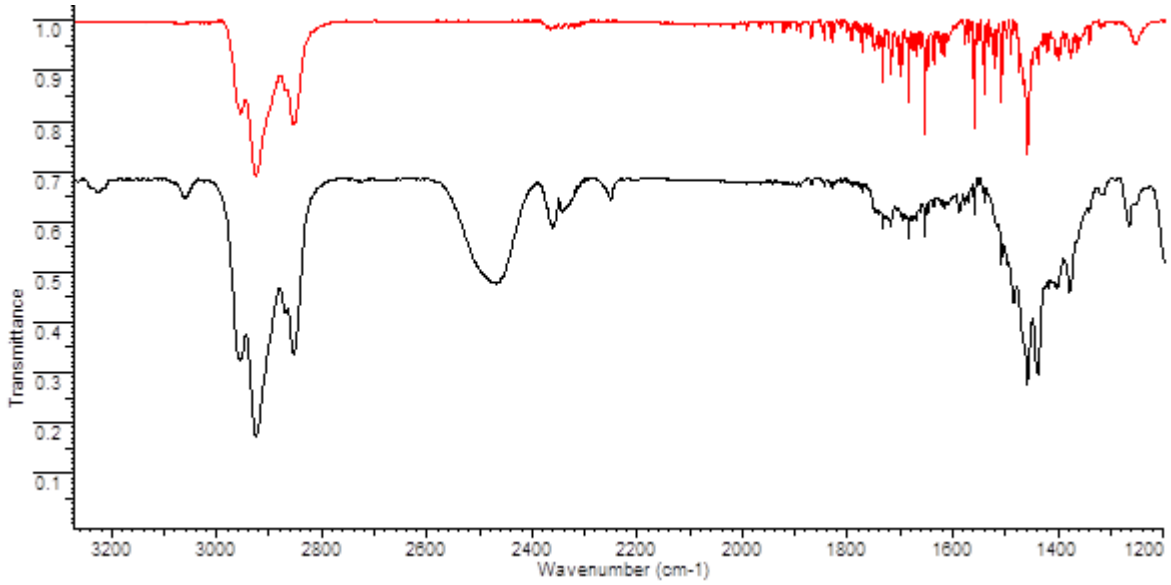

Figure S4. FT-IR spectra of PFCN2.5 (top) and PFCN2.5+B′(bottom).

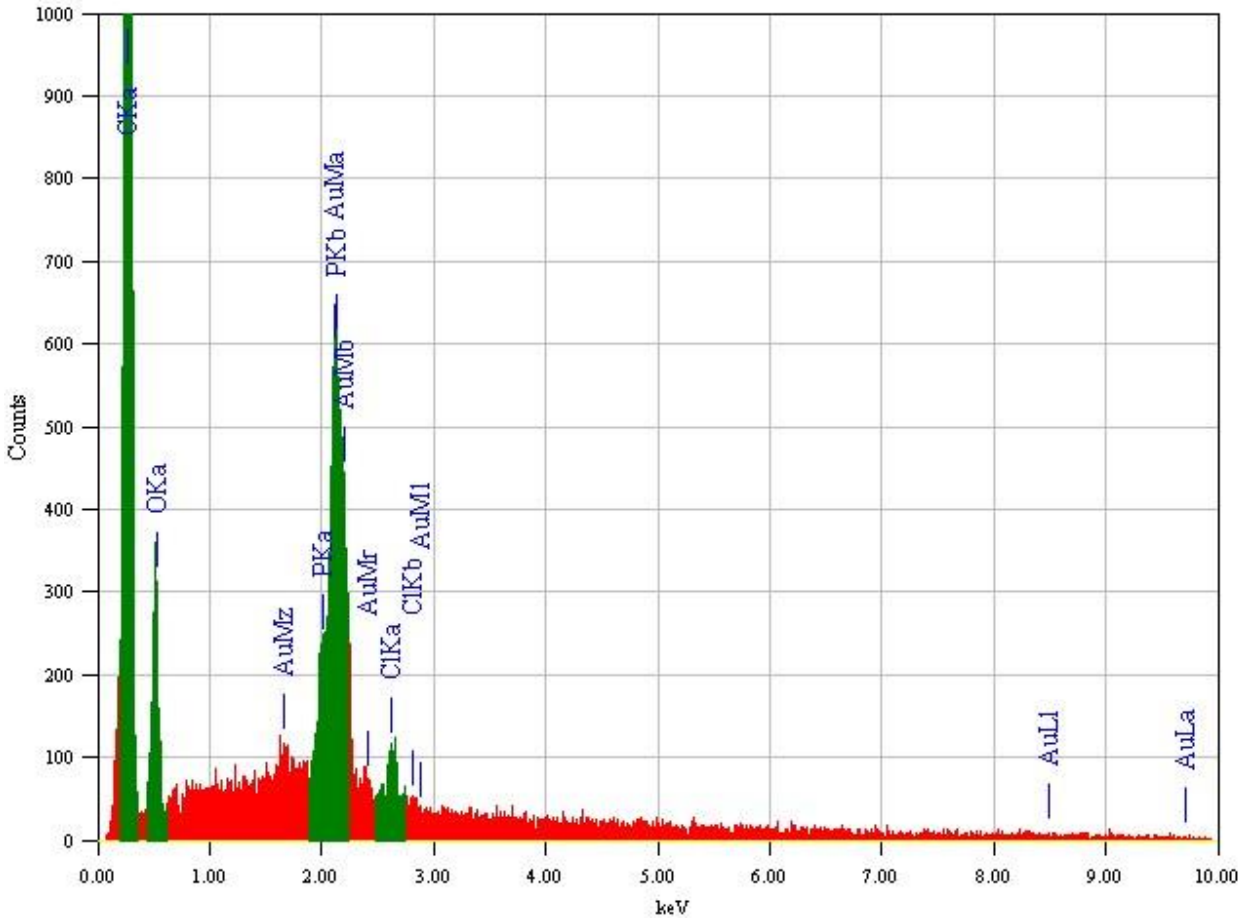

Figure S5. EDS for PFCN2.5+B′.

Table S3. UV-Vis and fluorescence spectral data for CPFs films.

CPFs	λ_{abs}, nm	λ_{em}, nm	Stokes shift, nm
PFCN0.5+B	386, 394*, 433*	498	65
PFCN0.5 [1]	385, 426*	499	73
PFCN2.5+B	383, 398*, 432*	465	33
PFCN2.5 [1]	385, 424*	463	39
PFCN5+B	383, 395*	527	132
PFCN5	383, 394*	530	136

* Shoulder

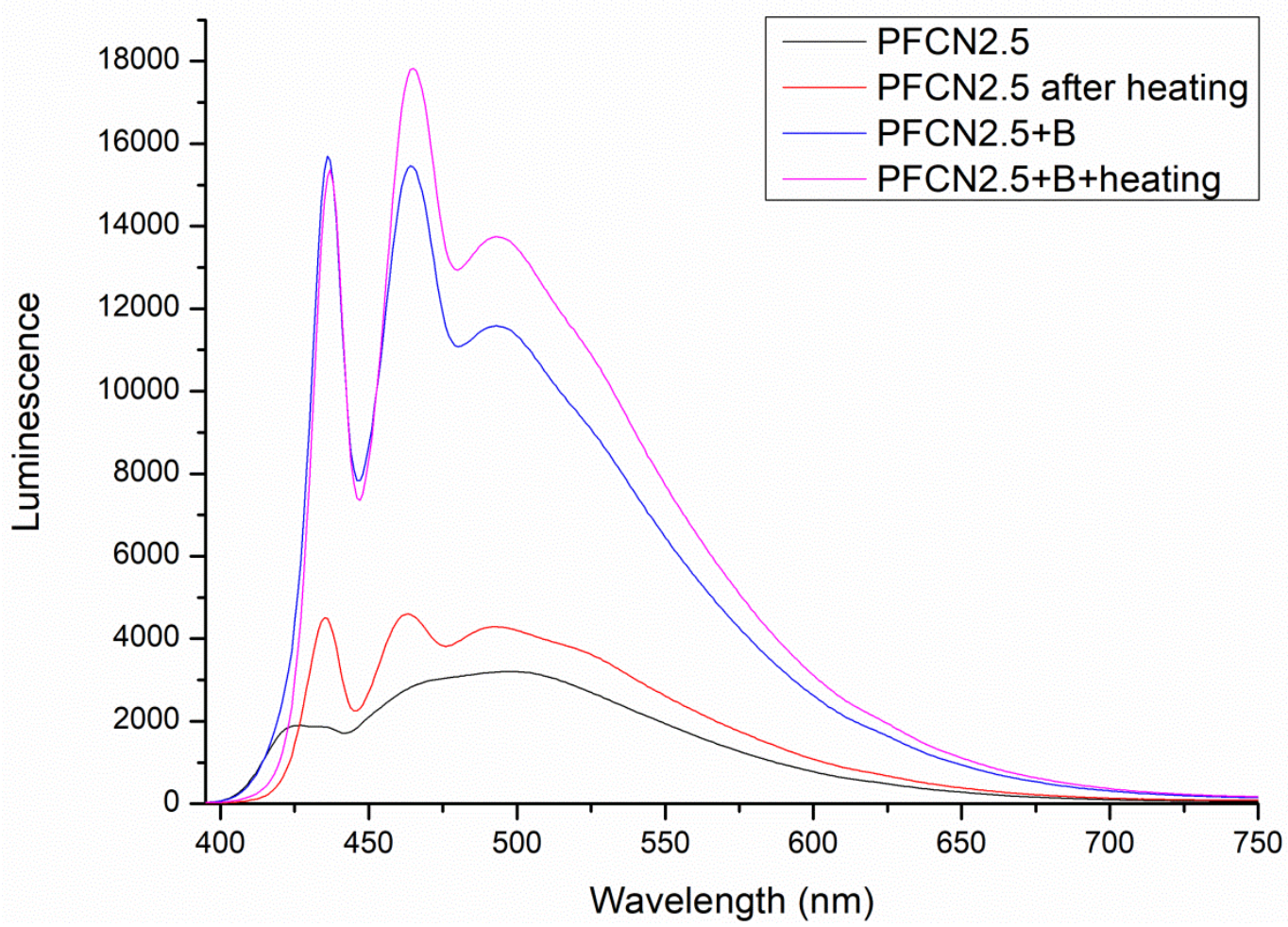

Figure S6. PL spectra of PFCN2.5, PFCN2.5+B, PFCN2.5 after heating at 80°C for 4 h, and PFCN2.5+B after heating at 80°C for 4 h in films.

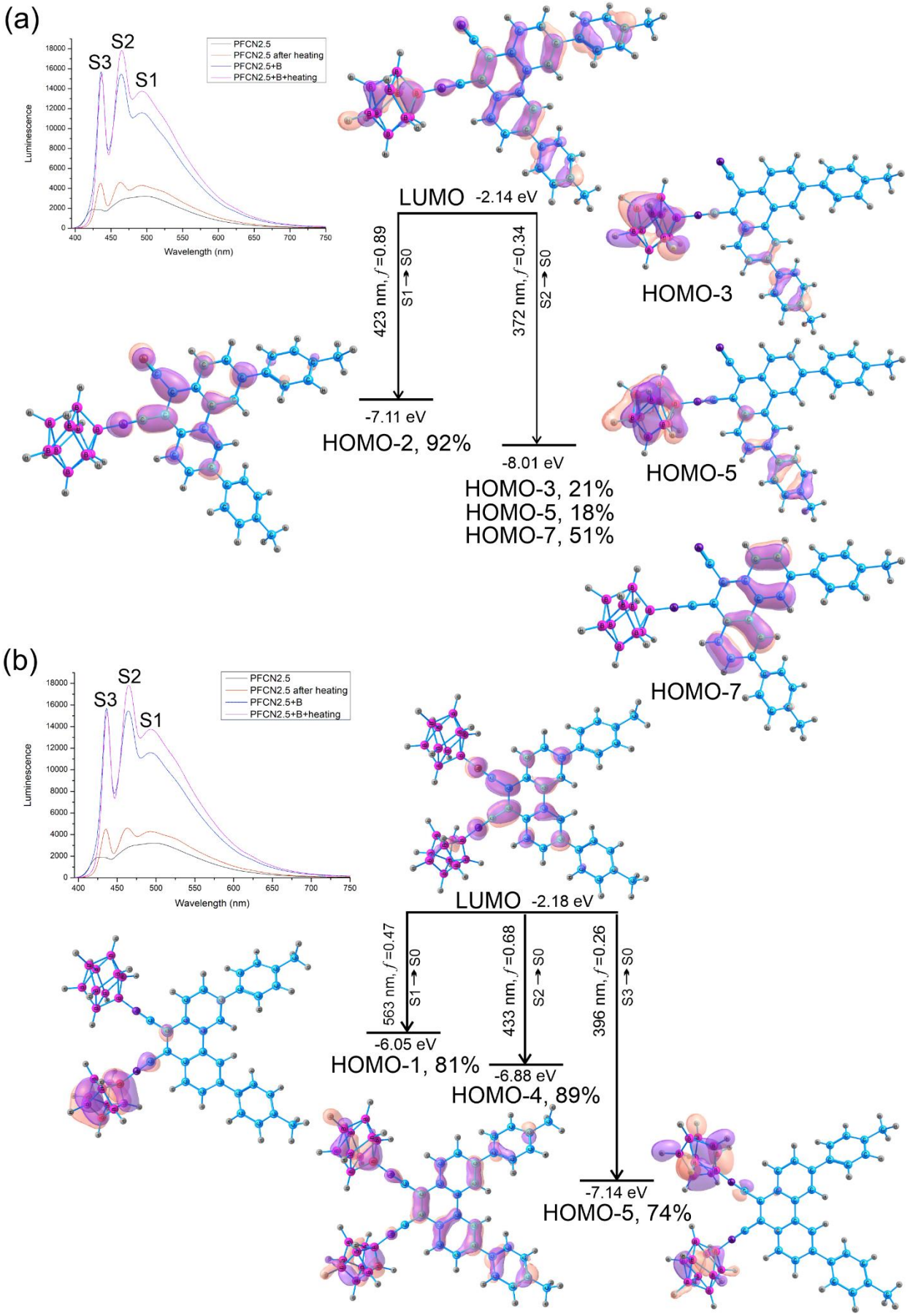

Figure S7. Transition scheme and molecular orbitals in the excited state of molecules. (a) Molecular orbitals of the PFCN-B1; (b) Molecular orbitals of the PFCN-B2 molecule. Transition maxima in the luminescence spectrum according to Table 1 (main text). Energy of molecular orbitals in eV. The *f* is the oscillator strength. Maximum contributions of orbitals involved in this transition are given in percent (%). The inset shows the experimental luminescence spectrum.

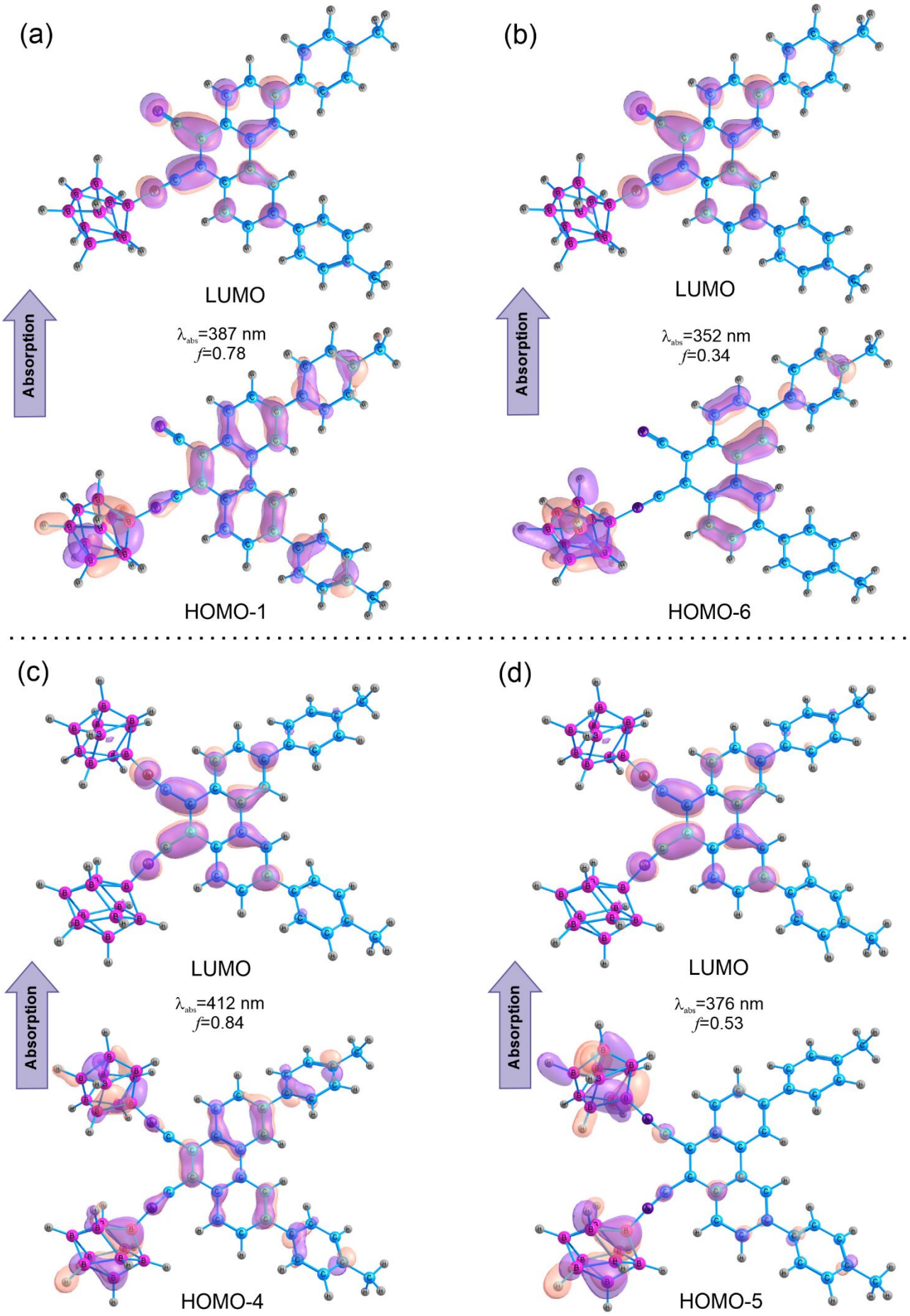

Figure S8. Molecular orbitals for the ground state of PFCN-B1 and PFCN-B2. (a) Molecular orbitals for the $S_0 \rightarrow S_1$ transition of PFCN-B1; (b) Molecular orbitals for the $S_0 \rightarrow S_2$ transition of PFCN-B1; (c) Molecular orbitals for the $S_0 \rightarrow S_1$ transition of PFCN-B2; (d) Molecular orbitals for the $S_0 \rightarrow S_2$ transition of PFCN-B2. The MOs according to Table 1 with the maximum contribution are indicated.

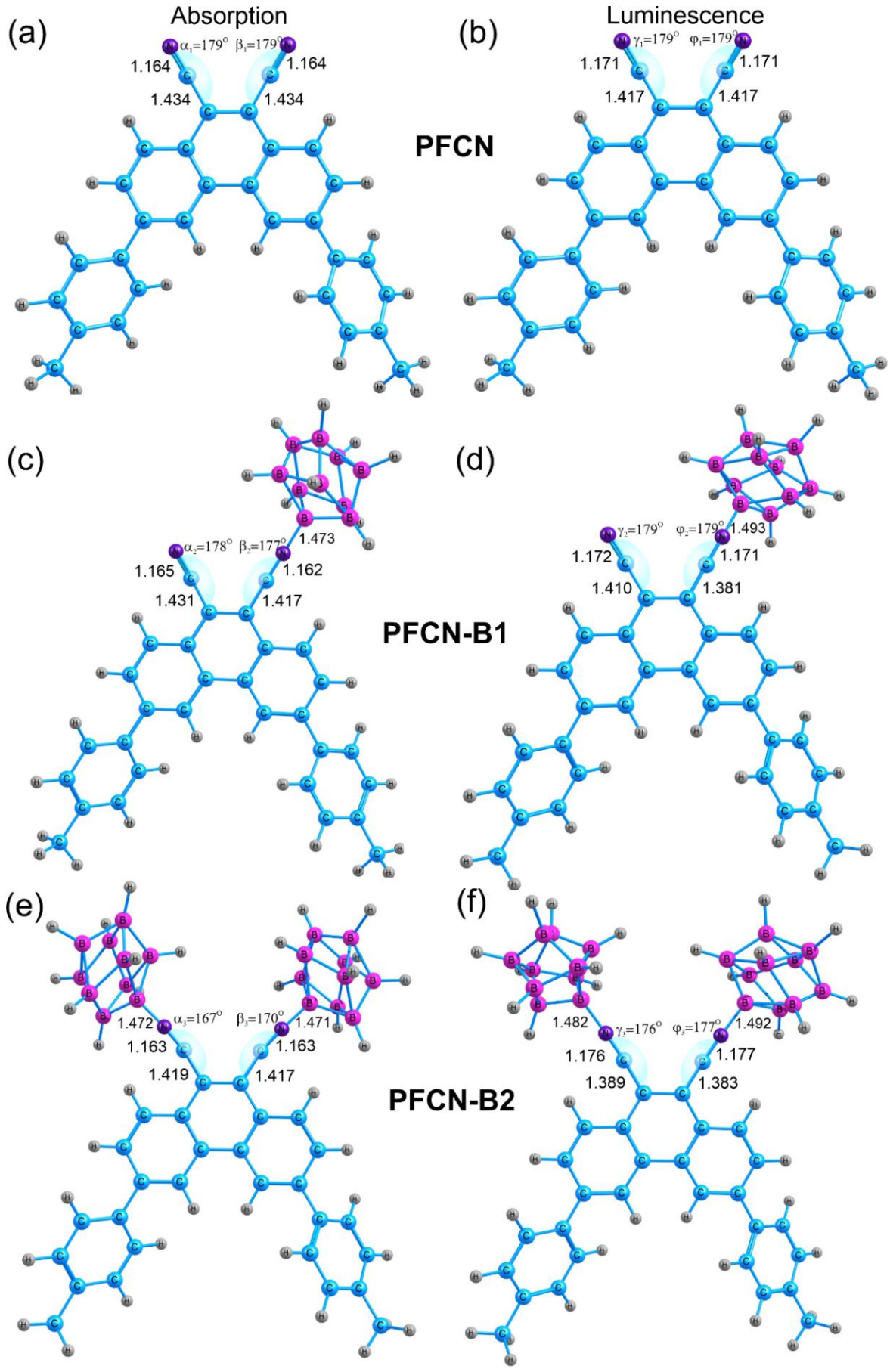

Figure S9. Geometry of the calculated molecules in the ground and excited states. Bond lengths (Å) and angles characterizing the change in spatial structure upon introduction of the boron cluster ($B_{10}H_9^-$) in the ground and excited states for different phenanthrene compounds. (a) PFCN geometry in the ground state; (b) PFCN geometry in the excited state; (c) PFCN-B1 geometry in the ground state; (d) PFCN-B1 geometry in the excited state; (e) PFCN-B2 geometry in the ground state; (f) PFCN-B2 geometry in the excited state.

Table S4. The calculated results of the excited states for PFCN-B1 and PFCN-B2, including the characteristics of the hole-electron distribution.

Transition	D (Å)	S_r	H (Å)	t(Å)	HDI	EDI
			PFCN-B1			
$S_1 \rightarrow S_0$	1.411	0.62	4.715	-2.033	3.92	7.07
$S_2 \rightarrow S_0$	1.563	0.51	4.402	-1.131	4.30	6.87
			PFCN-B2			
$S_1 \rightarrow S_0$	4.366	0.43	3.645	2.067	5.87	7.12
$S_2 \rightarrow S_0$	1.037	0.68	4.374	-2.147	3.75	6.82
$S_3 \rightarrow S_0$	4.299	0.35	3.909	1.656	5.54	6.93

Centroid distance index (D) is the distance between the hole and the center of mass of the electron (Å).
Overlap index (S_r) - is the degree of overlap between the holes and the electrons.
Width distribution index (H) is the average distribution range of electrons and holes (Å).
Degree of separation index (t) is the separation of electrons and holes (Å).
Hole delocalization index (HDI) is the degree of hole delocalization.
Electron delocalization index (EDI) is the degree of electron delocalization.
Used the Multiwfn program [2].

- The D-index, which corresponds to the large distance between the major hole and electron distribution regions, may indicate CT.
- The S_r-index at 0.55 (theoretical upper limit is 1.0) is a large value, meaning that about half of the holes and electrons are perfectly matched, indicating local excitation. As the value decreases, CT can be inferred.
- The H-index reflects the width of the average hole and electron distribution, the larger the value, the more significant the extent of the distribution. In the local region the H-indexes are small.
- Index *t* corresponding to negative values indicate that the degree of separation of holes and electrons in them is very small, with a positive value indicate a clear separation of holes and electrons, so it is more reasonable to consider these transitions as CT excitation.
- The HDI and EDI indices quantitatively characterize the uniformity of the spatial distribution of holes and electrons, respectively. Large calculated values indicate strong localization.

For the PFCN-B1 molecule, the D-index is 1.411 Å for the $S_1 \rightarrow S_0$ transition and 1.563 Å for the $S_2 \rightarrow S_0$ transition, indicating insignificant hole-electron displacement (Table S4). The H-index, which reflects the width of the average hole-electron distribution, has a significant range. The t-indexes corresponding to the $S_1 \rightarrow S_0$ and $S_2 \rightarrow S_0$ transitions have clearly negative values, indicating that the degree of hole-electron separation in them is very small. Comparing the isosurface maps of holes and electrons, it can be found that the HDI and EDI indices quantitatively characterize the uniformity of the spatial distribution of holes and electrons, respectively (Table S4).

For the PFCN-B2 molecule, the D-index for the $S_1 \rightarrow S_0$, $S_3 \rightarrow S_0$ transitions increases to 4.366 Å and 4.200 Å, respectively, relative to the indexes for the transitions of the PFCN-B1 molecule (Table S4). Thus, the larger the D-index, the larger the distance between the main distribution regions of holes and electrons, indicating CT. According to the H-index, the spatial extent of holes and electrons is wide. The t-index for $S_1 \rightarrow S_0$, $S_3 \rightarrow S_0$ has a positive value, indicating the clear separation of holes and electrons, so it is more reasonable to consider these transitions as CT excitation. In addition, S_r obtains a value of 0.43 for the $S_1 \rightarrow S_0$ transition and 0.35 for $S_3 \rightarrow S_0$, which may indicate CT (Table S4). However, for the $S_2 \rightarrow S_0$ transition, the D-index decreases to 1.037 Å and S_r increases to 0.68 compared to the other transitions. The t-index becomes negative, indicating that the degree of hole-electron separation is very

small in these transitions. Thus, this transition is a local excitation, which is well supported by the D, S_r and t indexes (Table S4) and the Λ diagnostic data.

The hole-electron contributions to each part of the molecules were studied, and a fragment-based heat map was constructed (Figures S10 and S11). For the PFCN-B1 molecule the system was divided into four fragments (Figure S10) and for the PFCN-B2 molecule into five fragments (Figure S11). The data obtained show that for the PFCN-B1 molecule, for the $S_1 \rightarrow S_0$ transition, 85.25% of electrons are located on fragment 4 (dicyanophenanthrene, Figure S10), while 26.72% and 24.76% of holes are located on fragment 3 ($B_{10}H_9$ cluster) and fragment 1 (*p*-tolyl), respectively. The degree of hole and electron overlap on fragment 4 is 56%. This means that the electron transfer during excitation is from fragment 3 and 1 to fragment 4. For the $S_2 \rightarrow S_0$ transition, 85.38% of electrons and 44.36% of the holes are located on fragment 4 (dicyanophenanthrene, Figure S10), and 41.08% of holes are located on fragment 3 ($B_{10}H_9$ cluster). This means that the excited electrons mainly come from fragment 3 and mostly move to fragment 4.

For the PFCN-B2 molecule, for the $S_1 \rightarrow S_0$ and $S_3 \rightarrow S_0$ transitions, more than 80% of electrons are located on fragment 5 (dicyanophenanthrene, Figure S11) and holes are located on fragment 3 ($B_{10}H_9$ fragment). The excited electrons come mainly from fragment 3, with most of them transferred to fragment 5 (dicyanophenanthrene). For the $S_2 \rightarrow S_0$ transition, 85.31% of electrons and 45.92% of holes are located on fragment 5 (dicyanophenanthrene, Figure S11), holes are located on fragments 3 and 4 ($B_{10}H_9$ clusters), more than 20% per fragment. Thus, the excited electrons come from fragment 5 and 3 (Figure S11) and remain on dicyanophenanthrene.

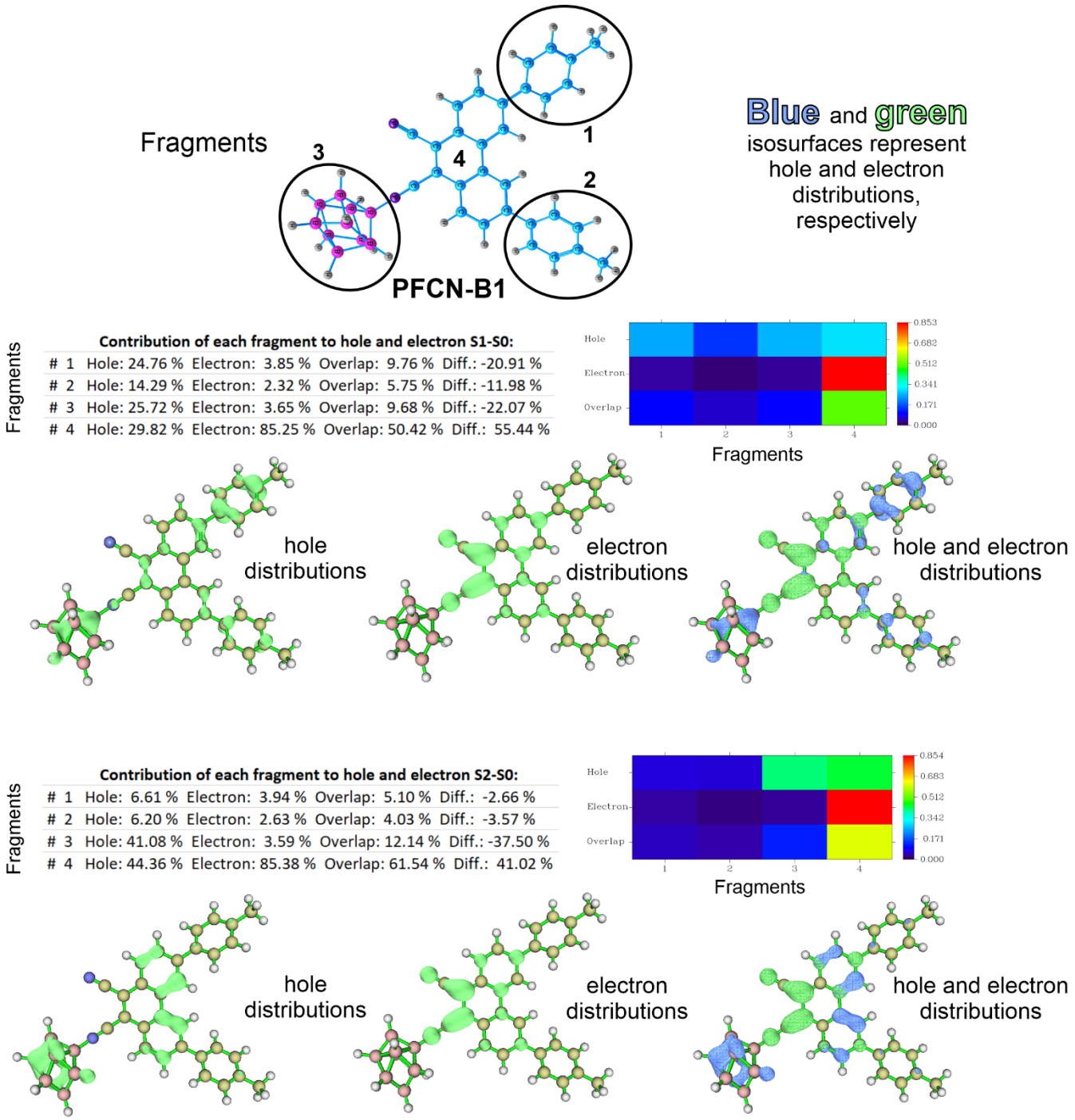

Figure S10. The PFCN-B1 molecular fragments electron excitation process analyzed by the hole-electron and interfragment charge transfer (IFCT) method. Contribution of different fragments of PFCN-B1 to the electron orbitals $S_1 \rightarrow S_0$ and $S_2 \rightarrow S_0$ states (%).

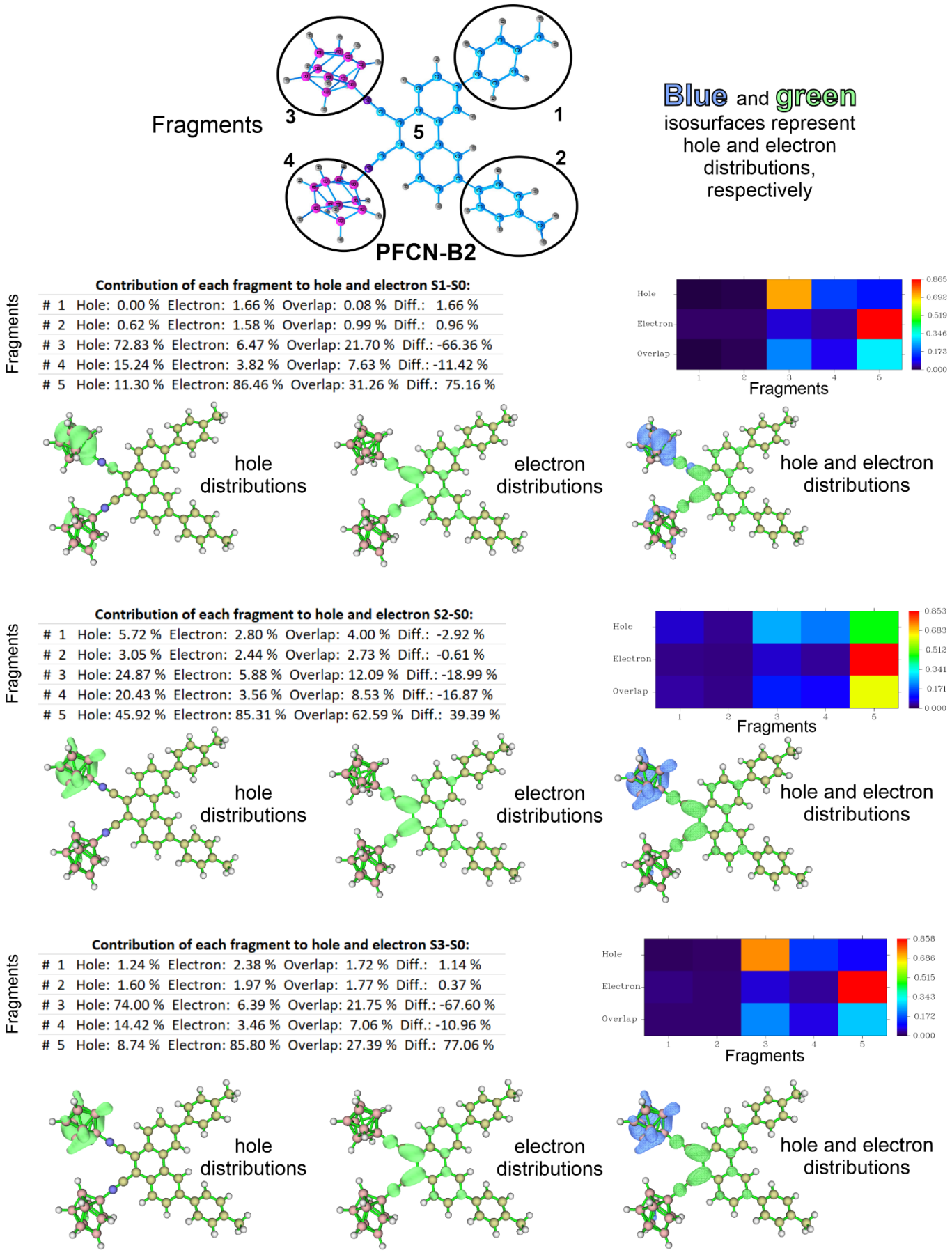

Figure S11. The PFCN-B2 molecular fragments electron excitation process analyzed by the IFCT method. Contribution of different fragments of PFCN-B2 to the electron orbitals $S_1 \rightarrow S_0$ $S_2 \rightarrow S_0$, $S_3 \rightarrow S_0$ states (%).

References

1. Yakimanskiy, A.A.; Kaskevich, K.I.; Zhukova, E. V.; Berezin, I.A.; Litvinova, L.S.; Chulkova, T.G.; Lypenko, D.A.; Dmitriev, A. V.; Pozin, S.I.; Nekrasova, N. V.; et al. Synthesis, Photo- and Electroluminescence of New Polyfluorene Copolymers Containing Dicyanostilbene and 9,10-Dicyanophenanthrene in the Main Chain. *Materials (Basel).* **2023**, *16*, 1–15, doi:10.3390/ma16165592.

2. Lu, T.; Chen, F. Multiwfn: A Multifunctional Wavefunction Analyzer. *J. Comput. Chem.* **2012**, *33*, 580–592, doi:10.1002/jcc.22885.